Comparison of Bremsstrahlung in the UCL Fast Simulation and GEANT4 for the Run IIb W Mass Measurement

1st Year Report

Tom Riddick
Supervisor: Dr. David Waters

June 3, 2008

Abstract

The validation of the UCL Fast Simulation model of Bremsstrahlung in the silicon tracker of CDF against the GEANT4 physics model by means of virtual test beam experiments is presented, and the subsequent modification of UCL Fast Simulation to better replicate the results of GEANT4 is detailed. Further validation exercises are considered.

Contents

1 Introduction

1.1 The Standard Model

The Standard Model [1] is a Quantum Field Theory that, put in naive terms, predicts the behaviour of all the known fundamental particles under the action of three of the four known fundamental forces, namely the strong, weak and electromagnetic forces[1]. While the Standard Model has a number of failings, most famously its apparent inability to be extended to include gravity[2], it has been proved extremely accurate within the scope of its validity.

The Standard Model consists of the amalgam of the field theories of the three different forces. The theory describing the electromagnetic force, Quantum Electrodynamics (QED) is extended by Glashow, Weinberg, Salam and Ward's theory of Electroweak Unification to include the weak force. The strong force is not (at least within the Standard Model) included in this structure of unification, but is perfectly compatible with it, and is covered by its own quantum field theory, Quantum Chromodynamics (QCD)[3].

Particles in the Standard Model [2] can be divided into fermions and bosons, depending on their spin. There are 12 fermions - the six leptons and the six quarks (matter is comprised of three of these, the up and down quarks and the electron). They are arranged into three doublets (also sometimes called families, or generations) in each case - see table 1. The particles exchanged during interactions between fermions comprise the bosons - see table 2. All of these have been observed experimentally except the Higgs boson.

$$\begin{pmatrix} u \\ d \end{pmatrix} \begin{pmatrix} c \\ s \end{pmatrix} \begin{pmatrix} t \\ b \end{pmatrix} \qquad \begin{pmatrix} e^- \\ \nu_e \end{pmatrix} \begin{pmatrix} \mu^- \\ \nu_\mu \end{pmatrix} \begin{pmatrix} \tau^- \\ \nu_\tau \end{pmatrix}$$

Table 1: The quark(left) and lepton (right) doublets.

Gauge boson	Symbol	Force
Photon	γ	Electromagnetic
Gluon	g	Strong
W boson	W^-/W^+	Weak
Z boson	Z^0	Weak

Table 2: The gauge bosons and the forces they correspond to.

1.2 Electroweak Physics

The weak interaction [2][3][4] started out as a point-like four-fermion coupling proposed by Fermi to explain nuclear β-decay. However it later became clear that it was not point-like, but instead merely very short ranged. This short range arose because the exchange particles of the weak

[1] Less naively, but possibly also less instructively, the Standard Model could be described simply as a quantum field theory that is observed in nature, of which the known particles are an emergent phenomena, and the forces seen as simply an attempt to describe in terms of mechanics the interaction terms of the field theory.

[2] While it might not be termed a failing, another important exception to the Standard Model is neutrino mixing, which is not predicted in the Standard Model, but is observed experimentally, giving us the first indications of high energy physics beyond the Standard Model.

[3] This interacts with the same quark matter field as the electroweak theory, linking them together into a single model to cover all three forces, the Standard Model, but this is not unification. Some extensions of the Standard Model, called Grand Unified Theories do unify all three forces, however there is presently no experimental evidence to vindicate these.

force, the W^+, W^- and Z^0 bosons[4], are all relatively massive, constraining the range over which a virtual weak boson exchange can take place. Their high mass also means high energies are needed to produce real weak bosons. This is in contrast with the massless photon, the exchange particle of the electromagnetic force.

The weak exchange bosons can interact with both quarks and leptons (and also with other electroweak exchange bosons). W boson vertices (Charged Current (CC) vertices) in Feynman diagrams either involve couplings between a charged leptons and its associated neutrino or between two quarks of different flavour. The coupling constant of leptonic CC interactions is universal, the same for all three lepton families and changes of lepton family at a vertex are forbidden.

For quarks, the situation is more complex. The quark eigenstates of the weak interaction are not the same as the mass eigenstates, instead three weak doublets are formed by unitary transformations among the quark doublets. This is parameterised in the CKM matrix. Flavour change then occurs within these weak couplets. The CKM matrix can accommodate two arbitrary complex phases; this allows us to introduce CP violation into the Standard Model. Two important (and related) aspects of the weak force are its CP violating nature and the V-A form of the weak interaction.

Z^0 bosons (mediators of the Neutral Current(NC)) cannot change quark flavor (nor can they change between lepton families), instead they can perform all the same interactions as photons, and in addition can form neutrino scattering and creation/annihilation vertices.

The early point-like theories of the weak interaction suffered from divergences at high energies, causing violations of unitarity (transition probabilities greater than one, clearly unphysical). These were solved by introducing the W boson, however this then generated new divergences, some in diagrams with all weak vertices, some in diagrams with a mixture of weak and electromagnetic processes (see figure 1 for examples of these). These could themselves be solved by introducing another neutral weak boson, the Z^0, which then added additional Feynman diagrams that cancelled out these divergences (see figure 2). In order for cancellations to occur between diagrams with both weak and electromagnetic vertices (such as diagram (b) of figure 1) and those with purely weak vertices (such as diagram (b) of figure 2), the electromagnetic coupling constant, e, must be roughly equal to the weak coupling constant, g. This then predicts the mass of the W and Z bosons to be on the order of 100 GeV. This parity between the weak and electromagnetic coupling constant led to the possibility of unification of the two forces. Glashow, Weinberg, Salam and Ward achieved such an electroweak unification in the late 1960's, introducing four electroweak quantum gauge fields upon combination of which you recover the photon, and a triplet of massless gauge bosons. The Higgs mechanism then allows for the three massless gauge bosons to be given masses, however it also introduces the as yet undiscovered Higgs boson.

The unified electroweak theory allows the W boson mass to be predicted with great precision; however it is dependent on a number of parameters, including the mass of the Z boson, α_{EM}, the mass of the quarks (especially the top quark) and most significantly it has a small correction dependent on the logarithm of the Higgs boson mass (from Higgs loop corrections such as figure 3) [5][5]. This means that, given we are able to accurately measure the mass of the W boson and constrain the other parameters with sufficient accuracy, we can make a prediction for the presently unknown and unpredicted Higgs boson mass. Figure 4 is a diagram showing how a combination of the mass of the top quark m_t and m_W can constrain the Higgs boson mass.

Predicting the Higgs boson mass is not the only reason to measure the mass of the W boson.

[4]The W^+ and W^- are antiparticles of each other, and hence often are referred to generically as the W boson.

[5]There is another, smaller, correction possible from supersymmetric particle loop corrections, if such things exist.

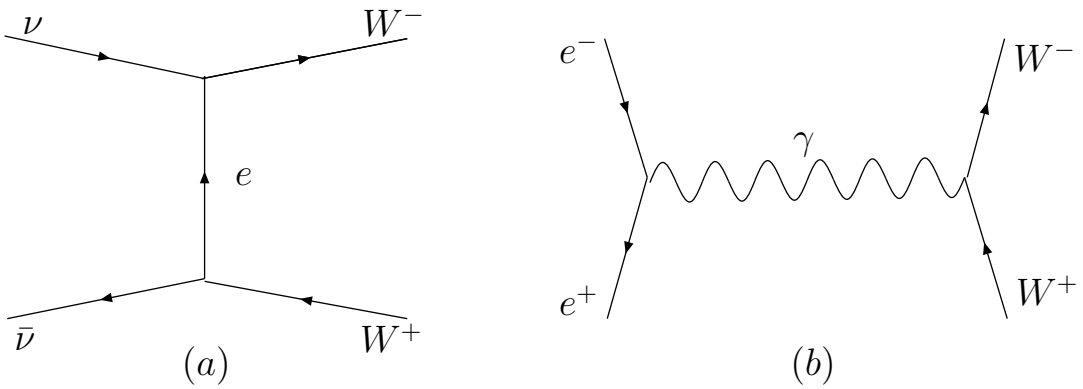

Figure 1: Divergent Feynman diagrams after the introduction of the W boson.

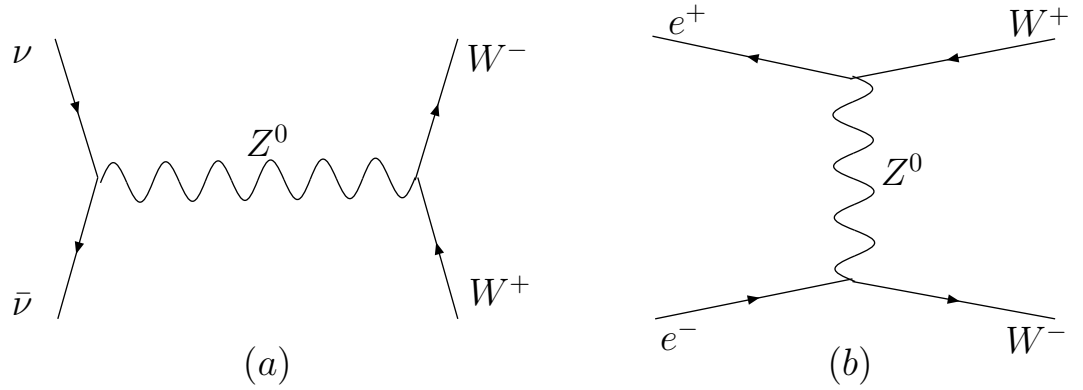

Figure 2: Diagrams that cancel divergences after the introduction of the Z boson.

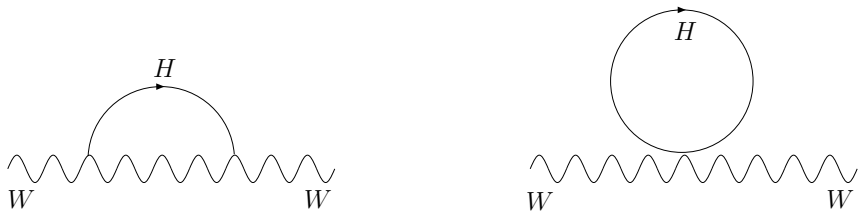

Figure 3: Single Higgs loop Feynman diagrams that contribute to the W boson mass.

Measuring the mass of the W boson provides a stringent test of the Standard Model and if the Higgs boson is discovered at the LHC as expected, we can compare the directly the measured Higgs boson mass with that derived indirectly from combining W boson and top quark mass measurements. Any statistically significant difference would point to new physics beyond the Standard Model. Measuring the W boson mass also provides valuable experience of making precision measurements at a hadron collider that could be carried forward to other precision measurements at the LHC.

1.3 Tevatron and CDF

The Tevatron is a proton - antiproton synchrotron that produces $\sqrt{s} = 1.8$ TeV collisions. These are studied at the two detectors on its ring, CDF and DØ. Tevatron began operation in 1985, and as befits the role of hadronic colliders at the high energy frontier as a discovery machine, in 1995 it discovered the top quark, completing the expected family of six quarks. It has also found evidence for $D^0 - \bar{D}^0$ oscillations, single-top, WZ and ZZ production, observed B_s oscillations and discovered the Σ_b [7].

However the Tevatron has also played a role in number of precision measurements. Although the high energy hadron collisions that occur produce a rather 'messy' detection environment compared to the leptonic colliders where such measurements are traditionally made, it has a number of advantages. Its high luminosity and long run time mean that a very large data set is now available, producing very high statistics and its high collision energy means that this is true even for relatively exotic processes. As both its detectors are general purpose, it has been possible to calibrate them against a wide range of different processes across its long period of operation, meaning the way they respond to any given signal is very well understood. All these factors have played a role in allowing the Tevatron to perform a number of very accurate measurements, which can only improve as it continues to produced yet more data. At leptonic colliders W boson parameters (mass and width) are harder to measure those of the Z boson because of their low production cross sections from lepton-antilepton collisions (single W boson production is not possible in a e^+e^- collision) and because they aren't produced at a given resonant energy like Z boson. This means that the Tevatron, while a hadron collider, can still make competitive measurements of W boson parameters. Furthermore, the systematic errors on such a measurement are largely uncorrelated with those on measurements from e^+e^- colliders, so the measurements will complement each other.

CDF II, Collider Detector at Fermilab II[6] [8], is one of the two general purpose detectors on the Tevatron ring. It is a multicomponent detector, see figure 5 for a schematic. The central section consists of a number of concentric layers of detector components arranged around the beam pipe. There are also two end-cap detectors, with layers arranged perpendicular to the beam pipe. The layers of the central section are, proceeding outwards, an inner silicon vertex detector, the Central Outer Tracker(COT), which is an open cell drift chamber, a layer of scintillators for time of flight analysis, the solenoid coil to provide the magnetic field in the COT, the central electromagnetic calorimeter (CEM), a hadronic calorimeter, steel shielding, and finally muon drift chambers. The arrangement of the end-cap detectors is similar. The combination of a high resolution tracker and calorimetry systems provides for excellent energy and momentum resolution on the tracks of leptons from W boson decay. The inner silicon vertex detector and time of flight scintillators are not used in the W mass analysis, though the passage of particles through them still has to be accounted for in simulations [5].

[6]CDF was upgraded at the same time as the Tevatron, CDF II refers to this upgraded detector.

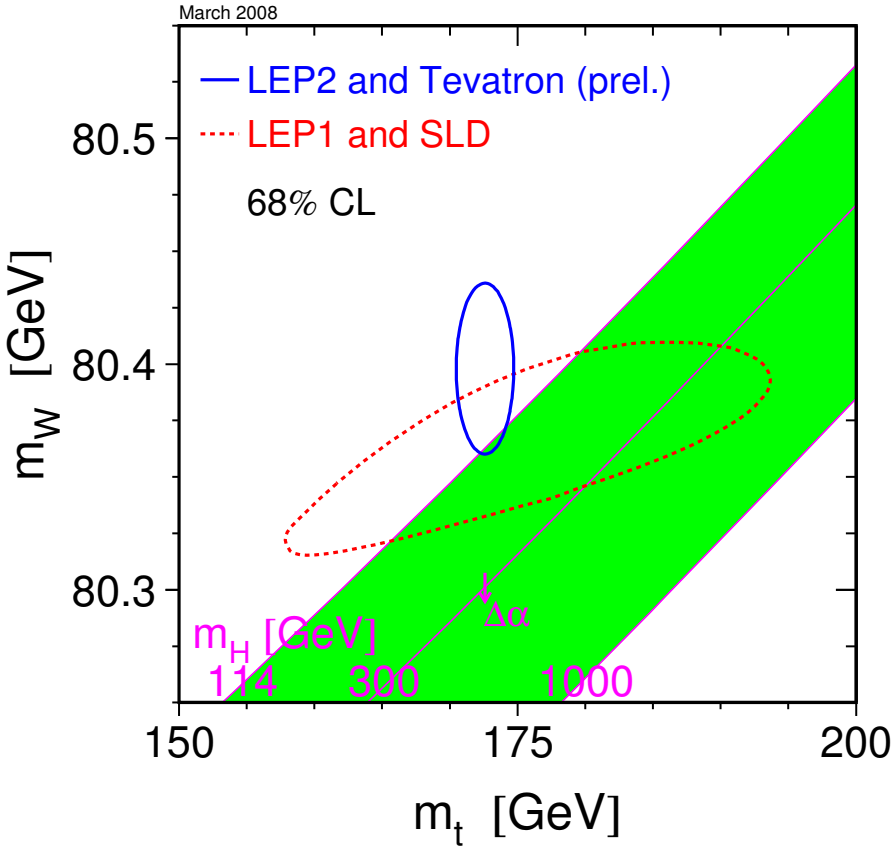

Figure 4: Diagram showing the 68% confidence level limit imposed on the Higgs boson mass through a combination of m_W and m_t by LEP-2 and the Tevatron (blue - by direct measurements of m_W and m_t), and LEP-1 and SLD (red - by indirect measurements of m_W and m_t). The upper edge of the green area is the lower bound on the Higgs boson mass imposed by direct searches at LEP. The lower edge of the green area is imposed as an upper bound on the Higgs boson mass, since for Higgs boson masses above 1 TeV, the SM and its formulae do not make sense. Reproduced from reference [6].

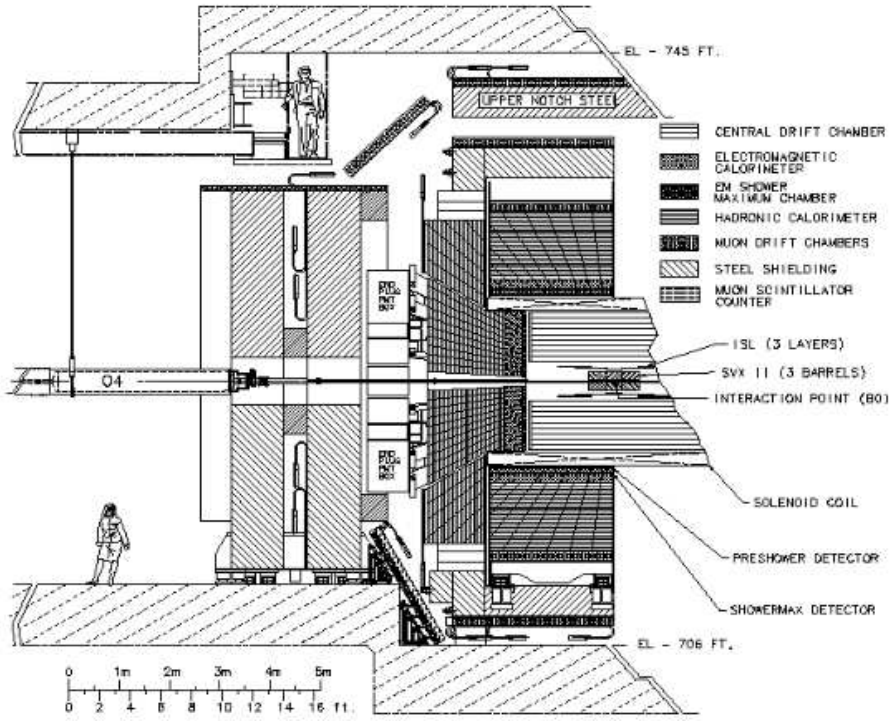

Figure 5: 'Elevation view' schematic of CDF II detector. Reproduced from reference [8].

1.4 W Mass Measurement

CDF is currently working on a measurement of the mass of the W boson, using 2.3 fb^{-1} of data taken during CDF Run II. This aims to be the most accurate measurement of the W boson mass to date.

W bosons are produced in $p\bar{p}$ collisions at the Tevatron mostly through the s-channel annihilation of u and d valence quarks, with a 20% contribution coming from sea quarks. They can either decay hadronically, or to a lepton-neutrino pair. Hadronic decays form jets, and are hard to measure accurately, especially given the large background of direct $q\bar{q}$ pairs, so are not considered in the W mass analysis, neither are decays to $\tau\nu_\tau$, as the τ will then decay to hadrons causing similar issues. Therefore the W mass analysis relies entirely on finding $e\nu_e$ and $\mu\nu_\mu$ pairs. Tight selection criterion are applied to the choice of candidate events to keep backgrounds to a minimum.

The escaping ν cannot be detected, neither can its momentum be inferred from missing momentum because the W will have an unknown p_z due to the unknown momentum fractions carried by the colliding quarks. This means the mass of the W boson, m_W cannot be reconstructed directly. The experimental strategy is therefore to calculate the quantity m_T, termed the 'transverse mass', which is given by

$$m_T = \sqrt{2p_T^l \not{p}_T (1 - \cos\Delta\phi)} \tag{1}$$

where $\Delta\phi$ is the angle between the missing momentum and the lepton in the transverse plane. The lepton's mass is taken as negligible.

Then a custom Monte Carlo simulation of $p\bar{p} \rightarrow W \rightarrow l\nu$ events is run, modelling their production, decay, and detection. These are used to generate theoretical distributions or 'templates' for the variable m_T for a range of values of m_W. The real m_T distribution from the data is then fitted to these templates, and the Poisson probability for each bin statistically to contain the number events observed, n_i, given the number expected, m_i is calculated and summed up to give an overall likelihood for a given template, $\mathcal{L}$, i.e.

$$\mathcal{L} = \prod_{i=0}^{N} \frac{e^{-m_i} n_i^{m_i}}{n_i!} \tag{2}$$

where i is an index over the N bins of the template in question. The best-fit value of m_W to the data is then that used to generate the template with the highest likelihood.

A custom Monte Carlo simulation of the detector (in fact two independent simulations are used, for cross-checking, the one used by the UCL part of the W mass working group is called UCL Fast Simulation) was chosen for this analysis instead of the standard GEANT-based CDF simulation. The advantages of UCL Fast Simulation are that computationally it can run much faster (about $O(10^4)$ times faster in terms of events/second) than the CDF simulation, and it allows much greater flexibility in the way the detector response is modelled. The high computational speed of UCL Fast Simulation allows for higher statistics studies of the production and decay of the W to be made, especially of the recoil model, and for calibration of the simulation against data from well constrained leptonic Z decays. The flexibility allows the effect of individual detector components to be studied separately.

However, despite these two advantages, it must be noted that UCL Fast Simulation has not undergone the same kind of rigorous validation that the widely respected GEANT4 toolkit[7] that is used in CDF simulation has [9], nor does it use as detailed a modelling of the various physics processes that particles undergo as they pass through the CDF detector. The purpose

[7]GEANT4 is toolkit for modelling particle detectors, used throughout the particle physics community.

of this validation exercise is hence to check the performance of UCL Fast Simulation against GEANT4 in simulating various physics processes. The first process to be validated was electron Bremsstrahlung in silicon, the results of which are presented in the rest of this report along with details of the subsequent modification of UCL Fast Simulation to better reproduce the results of GEANT4. Given that the electron carries most of the information about the W boson mass in any given electron candidate event, accurate modelling of electron Bremsstrahlung is of great importance.

The current W mass analysis at CDF builds on a recent measurement of the W width [10], and before that a prior measurement of W boson mass at CDF with less data. The later of these is detailed at some length in reference [5], which reviews many of the principles of the current W mass analysis in far more depth than given here.

2 Passage of Particles Through Matter

2.1 Electrons

Electrons can lose energy in matter through three processes - Møller scattering, ionisation and Bremsstrahlung (for positrons the processes are Bhabha scattering, ionisation, Bremsstrahlung and positron annihilation)[11]. The relative magnitude of these varies with the energy of the incoming electron. For this analysis we are typically interested in electrons with energies from tens of GeV down to hundreds of MeV. Higher energy electrons cannot be produced by W/Z boson decay so are of no interest to us. Lower energy electrons (in the MeV range) tend to be irrelevant to the accuracy of the analysis - they are unlikely to be the primary daughter particle produced by a W/Z decay event, are unlikely to be significant given the multitude of low energy hadronic recoil tracks and often are swept up by the magnetic field of the COT and don't reach the calorimeter.

Within this range of energies of interest, Møller scattering (and for positrons, Bhabha scattering and Positron annihilation) are completely negligible. Bremsstrahlung is by far the dominant process, while ionisation has a small, but potentially significant contribution, particularly at the lower end of this energy range - see figure 6. Hence during this analysis the processes of interest were Bremsstrahlung and ionisation.

2.2 Electron Bremsstrahlung

An electron cannot radiate a photon in a vacuum because such a process cannot conserve both energy and momentum. However when an electron passes through an atom, it is accelerated and decelerated by the electric field of the nucleus (the electric field of the atomic electrons can also have an affect), causing it to lose energy by radiating photons. The nucleus recoils in this process, allowing energy and momentum to be conserved. This process is called Bremsstrahlung (meaning 'braking radiation' in German) [3]. The dominant Feynman diagrams for this process are shown in figure 7. Note that they are closely related to those for pair production.

The total cross section for Bremsstrahlung is already reasonable well described in UCL Fast Simulation, and of little concern to us here. What is of interest is the differential cross section for Bremsstrahlung as a function of the variable y, which is the fractional energy lost by the electron through the radiation of photons, i.e.

$$y = \frac{k}{E} \tag{3}$$

where E is the energy of the incident electron, k the energy of the radiated photon. While this can be derived from first principles with a variety of different approximations [12][13], most

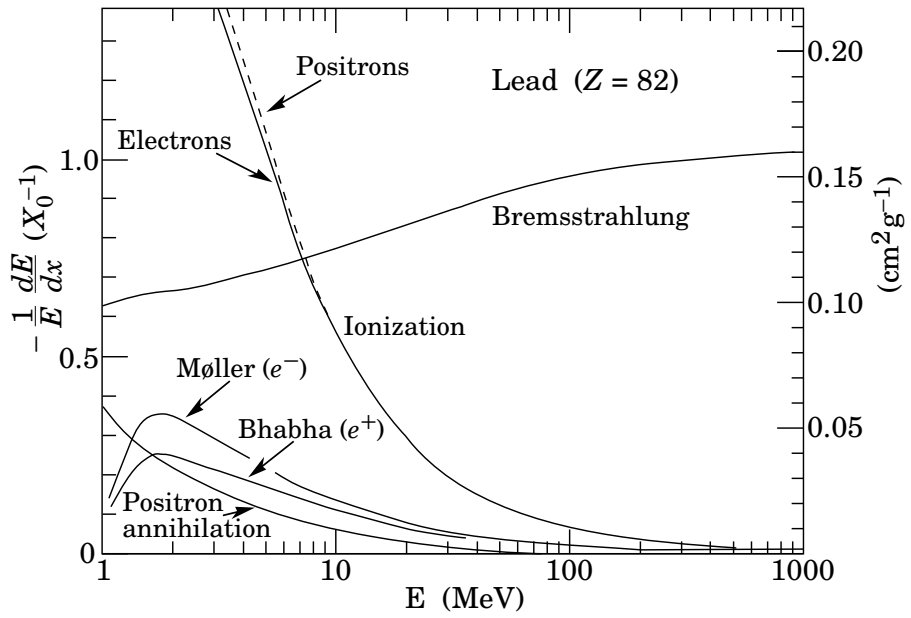

Figure 6: The fractional energy loss per radiation length in lead as function of electron energy. Reproduced from Figure 27.10 of reference [11].

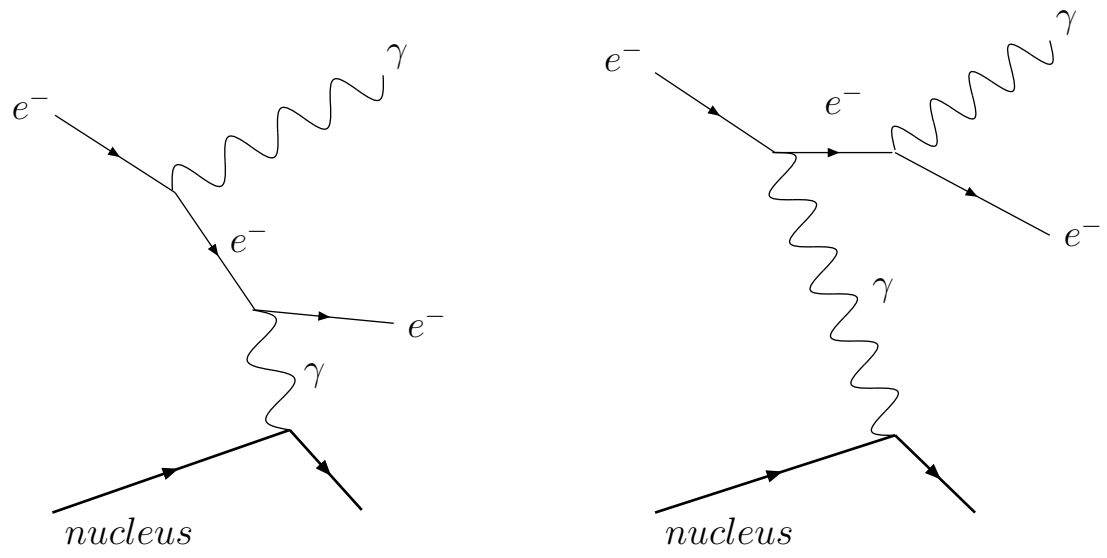

Figure 7: The two dominant Bremsstrahlung Feynman diagrams.

of these are quite algebraically involved and beyond the scope of this analysis, hence are not reproduced here. Instead I propose to start from the most basic approximate functional form, and discuss how this can be expanded upon, mostly motivated by GEANT4's implementation [14] but also with reference to the literature.

The most basic functional form for the Bremsstrahlung y spectrum at high energies (given in review [11]) is

$$\frac{d\sigma}{dy} = \frac{AE}{yX_0N_A}\left(\frac{4}{3} - \frac{4}{3}y + y^2\right). \tag{4}$$

where A is the atomic mass number of the absorber, X_0 is the radiation length of the absorber and N_A is Avogadro's number. It must be noted that this formula is based on many assumptions and will be inaccurate near $y = 1$ and $y = 0$. The inaccuracy near $y = 1$ is because equation 4 assumes that the screening of the nuclear Coulomb charge by the atomic electrons is complete (i.e. the reduction in strength of the nuclear Coulomb field acting on the electron due to the screening always takes it maximum value), but a very high y this may not be true. The inaccuracy near $y = 0$ is due to two effects - dielectric suppression and the Landau-Pomeranchuk-Migdal (LPM) effect. Note equation 4 is actually a simplified version of the 'Complete Screening Formula' given in reference [13], in the former a small term that doesn't scale with radiation length is discarded for convenience. This may also contribute to inaccuracies at high-y.

The LPM effect is due Bremsstrahlung interactions at low-y being spread across a relatively long distance, this being possible because the momentum transfer is smaller, allowing the virtual exchange particle a relatively long life. The distance the interaction is spread over is called the formation length. If this becomes comparable with the distance between scattering centres (i.e. atomic nuclei) then quantum interference can occur between the amplitudes for Bremsstrahlung at different centres [11]. The LPM effect only becomes important for Bremsstrahlung interactions with a y below a certain threshold, which is given by [15]

$$y < \frac{E}{E_{LPM}}. \tag{5}$$

Here E_{LPM} is dependent on the radiation length of the material in question, and is given (in eV) by $E_{LPM} = 3.8 \times 10^{12} X_0(\text{cm})$. For energies below this value, the Bremsstrahlung differential cross section is suppressed by a factor of S_{LPM}. A good approximation for this is given by

$$S_{LPM} = \sqrt{\frac{kE_{LPM}}{E^2}} \tag{6}$$

This is the equation used for the value of S_{LPM} in both GEANT4 and the UCL Fast Simulation. It gives values that are within about 10% of a more detailed calculation performed by Migdal [16][15].

UCL Fast Simulation (similar to [10]) adopts equation 4 as its y spectrum, but also accounts for the LPM effect. Each layer of silicon in the UCL Fast Simulation is split into 4 sub-layers, and as an electron passes through each sub-layer a number of Bremsstrahlung photons are generated randomly according to a Poisson distribution with a mean based upon the total cross section for Bremsstrahlung in the material; this usually gives either zero or one photon, although multiple photon emission is possible. The energy of any generated photons is randomly sampled from equation 4. If the generated y is below the LPM threshold (according to inequality 5) then an LPM suppression is applied. This suppression is made by generating a random number in the range zero to one, if this is greater than the LPM suppression factor S_{LPM} given by equation 6 then the photon is discarded. Any remaining photons are then propagated separately henceforth, and their energy is deducted from that of the electron.

GEANT4's implementation [14], in terms in physics, differs from that of the UCL Fast Simulation in two respects. Firstly it samples photon energies from a more sophisticated y spectrum, better accounting for the possibility of incomplete nuclear screening and not discarding any small terms. Secondly it calculates the effect of dielectric suppression in addition to that of LPM suppression at low y values.

GEANT4 uses a parameterisation fitted to the y-spectra of Seltzer and Berger [12] for various elements[8]. The parameterization reproduces these tables to on average within 2-3%, at most differing by about 10%. For the case of incident electrons with energies higher than 1 MeV (which is the only case which we are interested in here), the parameterization is

$$\frac{d\sigma}{dk} = \frac{C}{k} \times \left((1 - a_h y)F_1(\delta) + b_h y^2 F_2(\delta)\right), \tag{7}$$

where

C : normalisation constant
k : photon energy
T, E : kinetic and total energy of primary electron
δ : Function of y given below.

The y dependence of equation 7 is not immediately obvious, given F_1 and F_2 are both complicated functions of y themselves through δ, though with knowledge of the kinetic and total energy of the electron[9] it can be calculated. F_1 and F_2 depend on the Z of the material in question (for silicon this is 14) and are given by

$$\delta = \frac{136 m_e}{Z^{1/3} E} \cdot \frac{y}{1-y}. \tag{8}$$

$$F_1(\delta) = F_0(42.392 - 7.796\delta + 1.96\delta^2 - F) \qquad \delta \leq 1 \tag{9}$$

$$F_2(\delta) = F_0(41.734 - 6.484\delta + 1.250\delta^2 - F) \qquad \delta \leq 1 \tag{10}$$

$$F_1(\delta) = F_2(\delta) = F_0(42.24 - 8.368 \ln(\delta + 0.952) - F) \qquad \delta > 1 \tag{11}$$

$$F_0 = 4 \ln Z - 0.55 (\ln Z)^2. \tag{12}$$

a_h and b_h are the parameters that are fitted to the results of Seltzer and Berger. They take the form:

$$a_h = 1 + \frac{a_{h1}}{u} + \frac{a_{h2}}{u^2} + \frac{a_{h3}}{u^3} \tag{13}$$

$$b_h = 0.75 + \frac{b_{h1}}{u} + \frac{b_{h2}}{u^2} + \frac{b_{h3}}{u^3} \tag{14}$$

where

$$u = \ln\left(\frac{T}{m_e}\right). \tag{15}$$

The 18 parameters a_{hi} and b_{hi} are second order polynomials in the variable

$$v = [Z(Z+1)]^{1/3}. \tag{16}$$

These parameters are given in the GEANT4 code. This parameterisation is similar to that of references [13][17]; the latter of these can be seen more clearly if you take the limit $a_h \to 1$, $b_h \to 0.75$, $T \to \infty$.

[8] These are themselves based on the synthesis of various theoretical results, they agree with theoretical and experimental results to within 5% for incident electrons with energies greater than 50 MeV.

[9] In fact T,E can be assumed to be the same at the energies we are interested in.

In addition to the LPM effect Bremsstrahlung is suppressed at low y by the dielectric effect. It is possible for Compton scattering of the radiated photons to take place during the Bremsstrahlung formation length (i.e. during the spread out Bremsstrahlung interaction). In the case this is forward Compton scattering, then the scattering can be coherent causing a shift in the photon's phase. If this phase shift is large across the formation length, then it will cause a loss of coherence, suppressing the photon emission [15].

GEANT4 uses the following parameterisation to calculate the suppression factor for the dielectric effect, S_p,

$$S_p = \frac{k^2}{k^2 + C_p \cdot E^2} \tag{17}$$

where,

$$C_p = \frac{r_0 \lambda_e^2 n}{\pi} \tag{18}$$

with

r_0 : classical electron radius
λ_e : electron Compton wavelength
n : electron density in the material.

This parameterisation (equations 17, 18) is nearly[10] identical to the formulation given in reference [15], although a little shuffling of constants is required to see this. While reference [15] compares this with experimental data and generally gets agreement within 5%, the conclusions of this paper are both disparate and complex, so it hard to tell if this confirms the form of equations 17 and 18.

The dielectric effect and LPM effect both act over the same length scale, the formation length, and it is incorrect to simply suppress the differential cross section by a combined factor of $S_p \cdot S_{LPM}$. Instead, according to the Physics Reference Manual of GEANT4 [14] they must be combined non-trivially using

$$\frac{1}{S} = 1 + \frac{1}{S_p} + \frac{S}{S_{LPM}^2} \tag{19}$$

to give S, the total suppression factor. This formula is derived in reference [18]. This can be solved to give

$$S = \frac{\sqrt{S_{LPM}^4 \cdot (1 + \frac{1}{S_p})^2 + 4 \cdot S_{LPM}^2} - S_{LPM}^2 \cdot (1 + \frac{1}{S_p})}{2} \tag{20}$$

This parameterisation of the low-y suppression is henceforth referred as parameterisation A. However it is not clear how GEANT4 applies this suppression factor, the manual [14] appears to indicate that, for emissions satisfying inequality 5 (i.e. below the LPM threshold), it performs a suppression by comparing S/S_p to a random number in the range zero to one, and discounting the photon emission if the random number is greater.

While examination of the GEANT4 code [19] confirms random number rejection procedure using S/S_p, and that S_{LPM} and S_p are calculated using equations 6 and 17, the way S is calculated in GEANT4 does not agree with equation 20 as given in the GEANT4 Physics Reference

[10] Equation 17 is indeed identical to equation 12 of reference [15]. However while the basic form of equation 18 appears to very similar to that given in reference [15], they don't appear to match exactly.

Manual[14]. The GEANT4 code instead gives the following formulation for calculating the value of S

$$S = \frac{\sqrt{w^2 + 4 \cdot S_{LPM}^2} - w}{\sqrt{w^2 + 4} - w} \tag{21}$$

with

$$w = S_{LPM}^2 \cdot (3 - S_p) \qquad \text{if } (1 - S_p) < 1 \times 10^{-6} \tag{22}$$

$$w = S_{LPM}^2 \cdot (1 + \frac{1}{S_p}) \qquad \text{otherwise.} \tag{23}$$

This parameterisation of the the low-y suppression is henceforth referred to parameterisation B. Notice that putting equation 23 into equation 21 gives the same numerator as equation 20. This formulation seems to have more sensible limits than equation 20, it approaches one as you approach the LPM threshold. No justification for this formulation has been found in the literature, and why GEANT4 differs from the implementation given in its manual is unknown. Furthermore it is not clear if there is a further factor due to dielectric suppression integrated into the GEANT4 code elsewhere. However, given the time constraints of the W mass analysis further investigation into this matter has not been undertaken.

3 UCL Fast Simulation Silicon Tracker Validation

3.1 Experimental Strategy

As discussed in section 1.4 the aim of this validation was to compare GEANT4 and the UCL Fast Simulation, and to modify the UCL Fast Simulation accordingly. Any improvements were to be cross-checked where possible with published theoretical models of Bremsstrahlung. This needs to be done without significantly slowing down the simulation. The total Bremsstrahlung cross section was not of immediate interest here as we fit for an overall material scale factor as part of the analysis, rather than overly rely on specific models of the total cross section. However as we only fit a single scale factor, the energy dependence of the total cross section still needs investigation - this has been earmarked as future topic of interest. Instead we want to investigate the fraction of energy that is given to radiated photons.

Rather than compare the simulation in the actual detector geometry of CDF in these two models, a virtual test beam experiment was setup for both models. This allowed us to compare the two models isolated from any other possible differences. Within each test beam experiment only a single physics process, Bremsstrahlung, would be simulated, all other process being disabled.

3.2 GEANT4 - Virtual Test Beam Experiment

A virtual test beam experiment was set up in GEANT 4.9.01.p01. This consisted of a 10 m square world volume, at the centre of which was placed a 10 cm square silicon plate in the x-y plane. The plate had a thickness of 1 mm. A test beam of 40 GeV electrons was fired at the plate along the z-axis, striking it at an angle of 90 degrees. Any electron and photon tracks passing more than 1 cm in the z direction beyond the centre of the plate were recorded (see figure 8). Each event consisted of the firing of one electron and the tracking of it and any secondary photons produced through Bremsstrahlung until they reach the edge of the world volume. To keep run times and file sizes to a minimum, no event information other than histograms was stored. The setup was extensively tested by displacing the position of the beam in the x-y

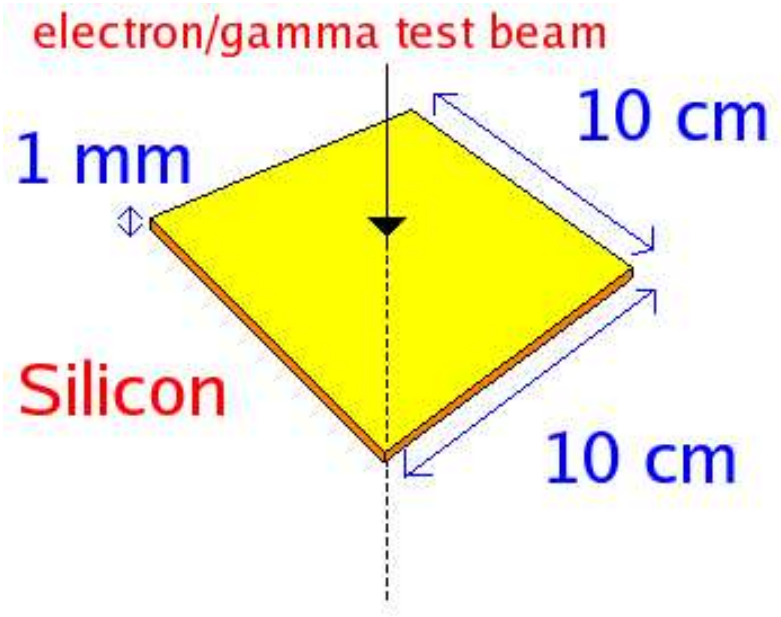

Figure 8: The setup of the virtual test beam experiment in GEANT4.

plane; no interactions were observed when the beam was displaced beyond the defined edges of the plate. Log file output showed that electrons were indeed passing through a thickness of 1 mm of silicon.

All physics processes in GEANT4 were disabled except for electron Bremsstrahlung. A number of histograms were defined and filled at run time, many of these - primary vertex energy, electron momentum, gamma momentum etc - simply confirmed the details of the experimental setup. The histogram most pertinent to this analysis was that of the differential cross section against y_{eff}, where y_{eff}, effective y, is defined as the fraction of the electron's energy radiated through the emission of photons, i.e for the emission of a single photon, y_{eff} equals y as defined by equation 3 and used throughout section 2.2. This was plotted on both logarithmic and linear scales. First the number of events against y_{eff} was histogrammed at run time. To correctly convert the logarithmic scale plot to one of differential cross section against y_{eff}, it was necessary to divide the content of each bin by the bin width. In the case of the linear histogram, events where no Bremsstrahlung occurred were not plotted, hence removing the dominant peak at y_{eff}.

It was observed from early plots that in total roughly 11% of the electrons underwent Bremsstrahlung while passing through the silicon plate. This was as expected from back of the envelope calculations based on the radiation length of electrons in silicon, and confirmed that 1 mm was, for Bremsstrahlung, a suitable choice of plate thickness. A significantly thicker plate would result in too many events with more than one photon being radiated that tends to skew the y_{eff} spectrum as will be seen later; a significantly thinner plate would mean a very large number of events would be needed to get satisfactory statistics.

To confirm that the output of GEANT4 was being interpreted correctly, a curve following the basic theoretical y spectrum given by equation 4 was overlaid on both the linear and logarithmic y_{eff} histograms. It was required that the overall constant of proportionality of equation 4 be determined to match the histogram scaling rather than calculated from theory. This was done by requiring that the integral of the theory curve and of the histogram matched in a region of good agreement (in terms of line shape). This determined, a good agreement was observed

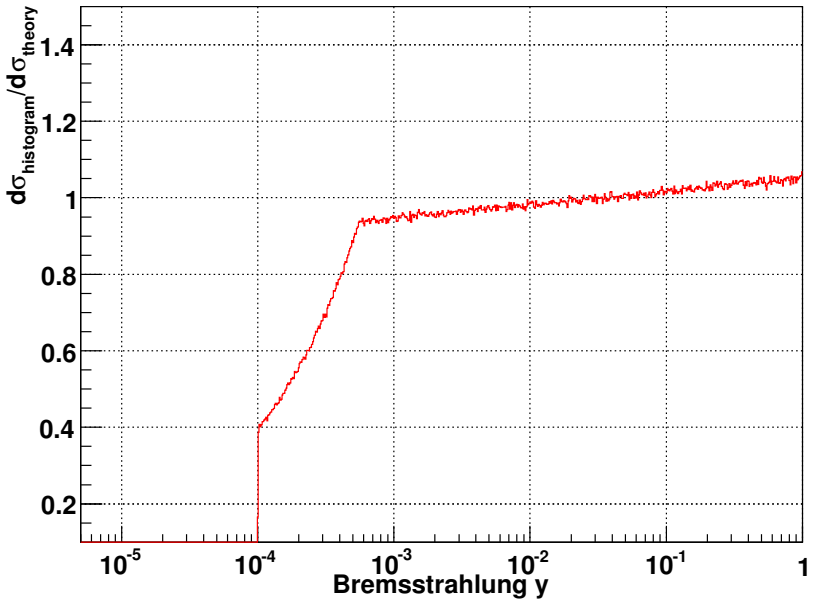

Figure 9: The ratio of UCL Fast Simulation Bremsstrahlung y_{eff}-spectra to the theoretical y-spectrum given by equation 4 on a logarithmic scale. Note the slight slope from $y = 1$ down to $y = 5.5 \times 10^{-4}$. In this region there is good agreement with the theoretical spectrum, the slope is due to multiple photon emission. At $y = 5.5 \times 10^{-4}$, the LPM cut-off is reached; below this value equation 4 proves inaccurate. The ratio is zero below $y = 1 \times 10^{-4}$ because this is the lowest value of y simulated in the UCL Fast Simulation.

between histogram and theory (see figure 11 in section 3.4), except at very high-y, and at low-y below the LPM cut off.

The value of y_{eff} for a given event is calculated by subtracting the energy of the electron after it has passed through the plate from its energy at the primary vertex (i.e. the set energy of the test beam). It was confirmed that this gave completely equivalent results to calculating y_{eff} by summing the energy of any photons radiated. It was also confirmed that if the test beam particle was changed to an e^+ exactly the same results where found.

3.3 UCL Fast Simulation - Virtual Test Beam Experiment

UCL Fast Simulation was modified to provide an analogous setup to that used in GEANT4. UCL Fast Simulation propagates lepton and photon paths through a series of layers - a series of silicon vertex tracker layers, the COT, the time of flight scintillators, the solenoid etc. This was modified by turning off all the layers but a single layer of silicon, and modifying this to be 1 mm thick. Then 40 GeV electrons were fired outward perpendicular to the silicon layer from the interaction point, one per event. The initial and final energy of the electrons was recorded, allowing y_{eff} to be calculated. Histograms of differential cross section against effective y were produced for both logarithmic and linear scales. Again it was confirmed that changing the test beam particle to an e^+ had no effect on the results.

Figure 9 was made by replacing the content of each histogram bin with the ratio $R = \frac{d\sigma_{\text{histogram}}}{d\sigma_{\text{theory}}}$, where $d\sigma_{\text{theory}}$ is taken from equation 4.

Note that even above the LPM cut off, the ratio plot of UCL Fast Simulation is not a

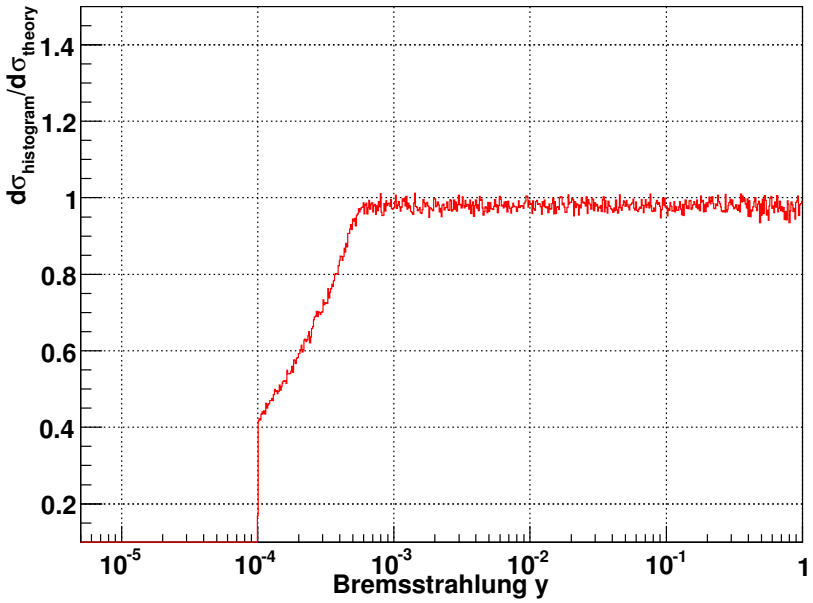

Figure 10: The ratio of UCL Fast Simulation Bremsstrahlung y_{eff}-spectra to the theoretical y-spectrum given by equation 4 on a logarithmic scale with no multiple Bremsstrahlung. Note the ratio is constant from $y = 1$ down to $y = 5.5 \times 10^{-4}$, indicating perfect agreement between the UCL Fast Simulation and equation 4 in this region. Below $y = 5.5 \times 10^{-4}$ equation 4 proves inaccurate and $y = 1 \times 10^{-4}$ represents the lowest value of y simulated by UCL Fast Simulation.

uniform distribution. The y we are plotting in histograms is an effective y, the total amount of energy that the electron has lost through photon emission, while the spectrum given by equation 4 is the spectrum for single photon emission. Secondary or further photon emission shifts events to higher y's than predicted by the single emission spectrum, while such events are reasonably rare, there are enough to give the ratio plot the observed slope. To confirm this, UCL Fast Simulation was run with only one simulation step being used in calculating the passage of the electron through the silicon, and any multiple emission events within this step re-assigned as single emission events. As can be seen in figure 10, an entirely uniform ratio plot was then observed in the appropriate region. This effect can also been seen in a plot of GEANT4 simulated data to the spectrum it follows, given by equation 7, but as you cannot manipulate GEANT4 in the same way to turn off multiple photon emission, you cannot test in the same way that this is due to multiple photon emission.

3.4 Bremsstrahlung Validation and Modification

In figure 11 the GEANT4 and UCL Fast Simulation y_{eff}-spectra are compared to the basic theoretical y-spectrum given by equation 4 (normalised against the GEANT4 histogram) on a logarithmic scale. The discrepancies at high-y and low-y were expected as UCL Fast Simulation samples from the spectrum given by equation 4, adding in LPM suppression at low-y, while GEANT4 samples from a more complex spectrum given by equation 7 and implements both LPM and dielectric suppression at low-y. In figure 12, the ratio $R = \frac{d\sigma_{\text{histogram}}}{d\sigma_{\text{theory}}}$ is shown for GEANT4 and UCL Fast Simulation, where $d\sigma_{\text{theory}}$ is taken from equation 4.

It was decided to modify UCL Fast Simulation such that it samples from equation 7 and so

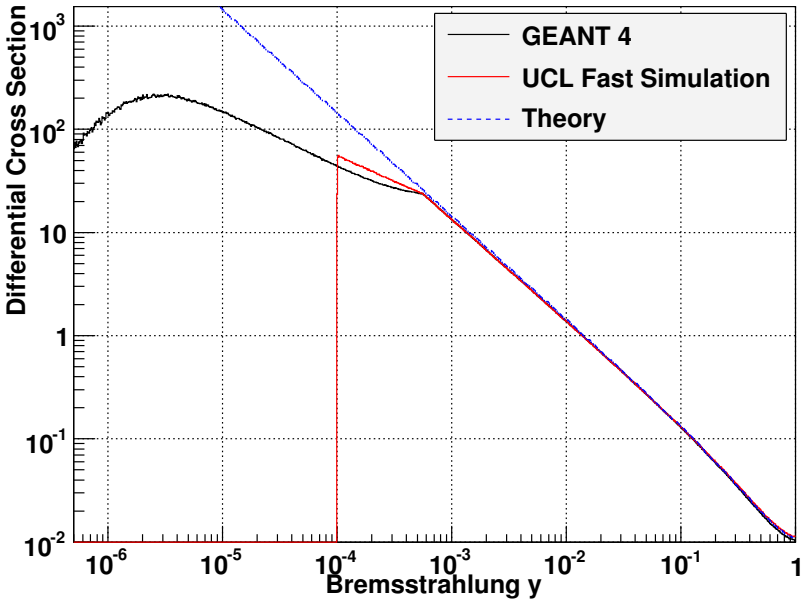

Figure 11: GEANT4 and UCL Fast Simulation Bremsstrahlung y_{eff}-spectra compared to a basic theory curve given by equation 4, on a logarithmic scale. Note the good agreement from $y = 1$ down to the LPM cut-off at $y = 5.5 \times 10^{-4}$, and the divergence of all three lines below this. The UCL Fast Simulation line is zero below $y = 1 \times 10^{-4}$, the minimum value of y simulated in UCL Fast Simulation.

that it uses a low-y suppression calculated by considering both the LPM effect and the dielectric effect. This was done in two stages. Firstly UCL Fast Simulation was modified to sample from equation 7, but keeping its original implementation of the low-y suppression, i.e. suppressed below the LPM cut-off (given by inequality 5) by a factor of S_{LPM}. Henceforth this is referred to as UCL Fast Simulation Modification A. In figure 13, the ratio $R = \frac{d\sigma_{\text{histogram}}}{d\sigma_{\text{theory}}}$ is plotted, where $d\sigma_{theory}$ is given by equation 4. It can be seen from this ratio plot that UCL Fast Simulation and GEANT4 now agree except in the low-y region. Both deviate from equation 4 at high-y.

Theory curves henceforth use the y-spectrum given by equation 7. Initial attempts to implement parameterisation A (see section 2.2) of the low-y suppression in a theory curve seemed to indicate that, despite being the method given in the documentation, the dielectric effect is not implemented in this fashion in GEANT4. Examination of the code proves this to be the case. The exact way that GEANT4 implements low-y suppression in the code is complex, and not fully understood by us. However, a satisfactory parameterisation based on the GEANT4 implementation was seen to be parameterisation B (see section 2.2), using equations 6, 17 and 21. Figure 14 shows R for GEANT4 and UCL Fast Simulation Modification A. Equation 7, with parameterisation B of low-y suppression is used for $d\sigma_{\text{theory}}$. Note there is a still a discrepancy between parameterisation B and GEANT4 below about $y = 5.5 \times 10^{-4}$ - the reason for this is unknown.

Adding the dielectric suppression as given by parameterisation B (see section 2.2) with equations 6, 17 and 21, to UCL Fast Simulation Modification A gives figures 15 and 16. The minimum value of y simulated was reduced to $y = 1 \times 10^{-5}$. This is henceforth referred to as UCL Fast Simulation Modification B. This eliminates the discrepancies at low-y down to about $y = 5 \times 10^{-5}$, although poor statistics and numerical fluctuations caused by the insufficient

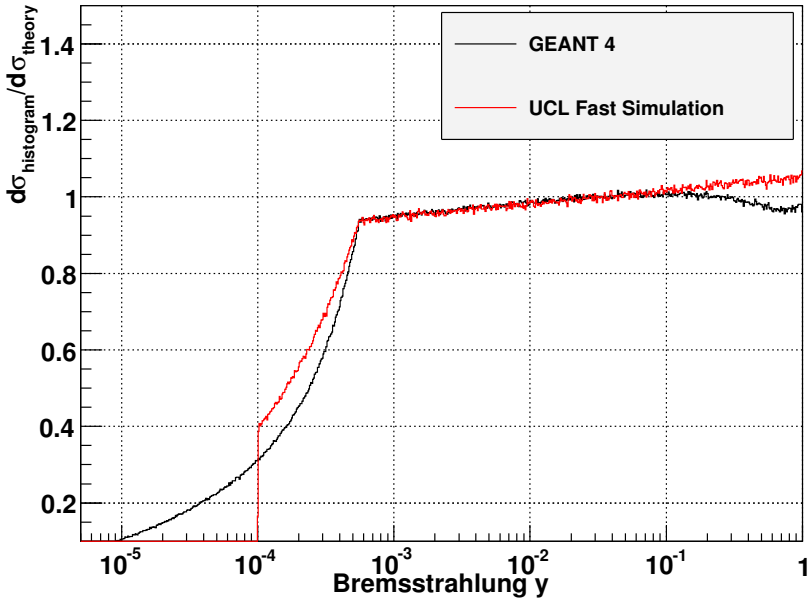

Figure 12: The ratio of GEANT4 and UCL Fast Simulation Bremsstrahlung y_{eff}-spectra to the theoretical y-spectrum given by equation 4 on a logarithmic scale. Note that above the LPM cut-off $y = 5.5 \times 10^{-4}$ UCL Fast Simulation's line agrees well with equation 4, displaying a slope due the possibility of multiple photon emission. GEANT4 also shows good agreement over this range, but deviates a little at high-y. Below $y = 5.5 \times 10^{-4}$ both GEANT4 and UCL Fast Simulation differ from equation 4. The UCL Fast Simulation line is zero below $y = 1 \times 10^{-4}$, the minimum value of y simulated in UCL Fast Simulation.

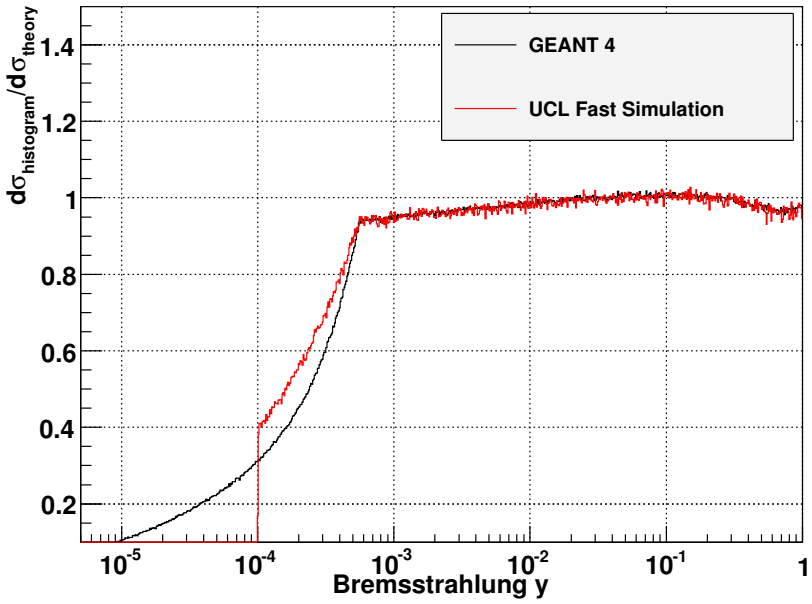

Figure 13: The ratio of GEANT4 and UCL Fast Simulation Modification A Bremsstrahlung y_{eff}-spectra to the basic theoretical y-spectrum given by equation 4 on a logarithmic scale. Note the good agreement between GEANT4 and UCL Fast Simulation Modification A above $y = 5.5 \times 10^{-4}$, including in the very high-y region. Both curves deviate from equation 4 at very high-y. Below $y = 5.5 \times 10^{-4}$ disagreement still occurs between GEANT4 and UCL Fast Simulation, and both deviate from equation 4.

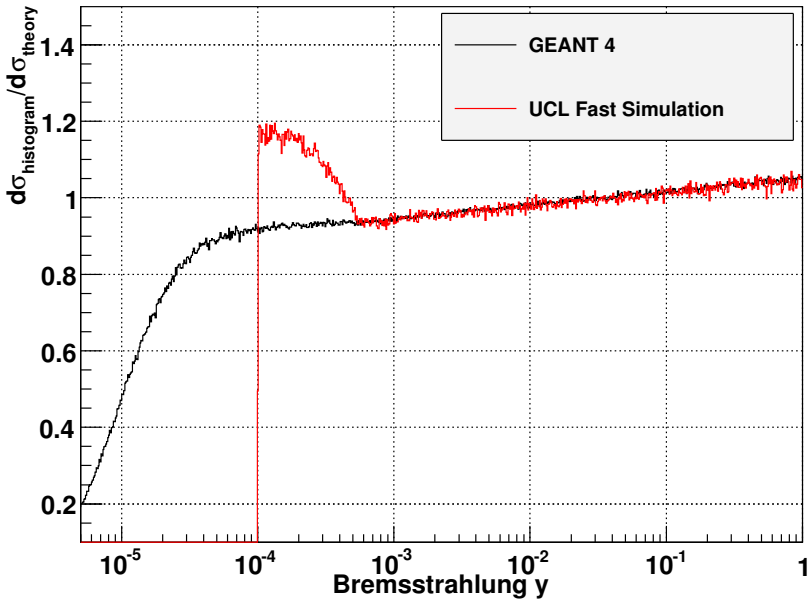

Figure 14: Ratio of GEANT4 and UCL Fast Simulation Modification A Bremsstrahlung y-spectra to an advanced theoretical y-spectra given by equation 7 and using parameterisation B for low-y suppression. Note the agreement of GEANT4 and UCL Fast Simulation Modification A above the LPM cut-off (the slope being due to the possibility of multiple photon emission), the deviation of UCL Fast Simulation Modification A below the LPM cut off from the GEANT4 results, and the deviation of GEANT4 below $y = 5.5 \times 10^{-4}$ from a ratio of one.

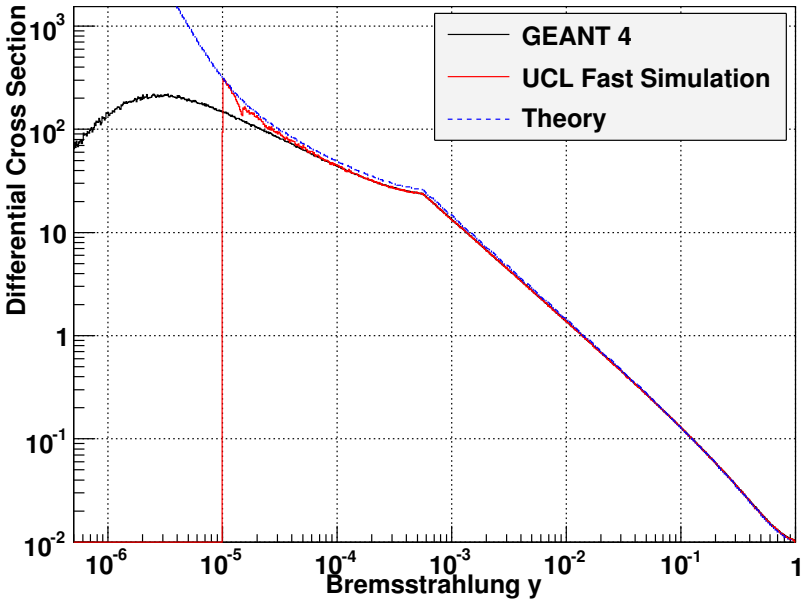

Figure 15: GEANT4 and UCL Fast Simulation Modification B Bremsstrahlung y_{eff}-spectra, compared to an advanced theory curve given by 7 with parameterisation B used for low-y suppression, on a logarithmic scale. Note the good agreement between GEANT4 and UCL Fast Simulation Modification B in the range $y = 5 \times 10^{-5}$ to $y = 1$, both above and below the LPM cut-off.

integration points during the integration of equation 4 add a lot of noise to the ratio plot at low-y. Hence we have good agreement between UCL Fast Simulation Modification B and GEANT4 in the range $y = 1$ to $y = 5 \times 10^{-5}$ but below this value we observe a discrepancy of unknown origin. Note that the actual number of events producing y values below 5×10^{-5} is not great, as can be seen in figure 17, which shows the absolute number of events against y_{eff}. Therefore it is expected that this unresolved deviation will have a negligible effect on the W boson mass measurement. This will be further investigated in section 3.5.

Note for the purposes of this validation exercise UCL Fast Simulation Modification B was set to simulate values of y down to $y = 1 \times 10^{-5}$, however the final version of the code to be used in the W mass measurement is likely only to simulate values of y down to $y = 5 \times 10^{-5}$, the point below which it no longer accurately reproduces the results of GEANT4. The effects of this cut-off are considered in section 3.5.

3.5 Systematic Error on the W Mass Measurement

The fitting of E/p distributions is central to the W mass analysis. Any photons that are radiated in the silicon vertex detector will reduce the measured value of electron momentum, p, but will be picked up in the electromagnetic calorimeter so will not reduce the measured E, changing the measured E/p. This should be modelled in UCL Fast Simulation but any errors in the modelling of Bremsstrahlung will effect the simulated distribution E/p. This will result in slight errors in the E/p fitting, that will propagate directly to the W mass. Hence it is important to estimate the effect the accuracy of UCL Fast Simulation's modelling of Bremsstrahlung will have on the accuracy of the measured m_W.

To do this we run multiple versions of UCL Fast Simulation Modification B. One version will

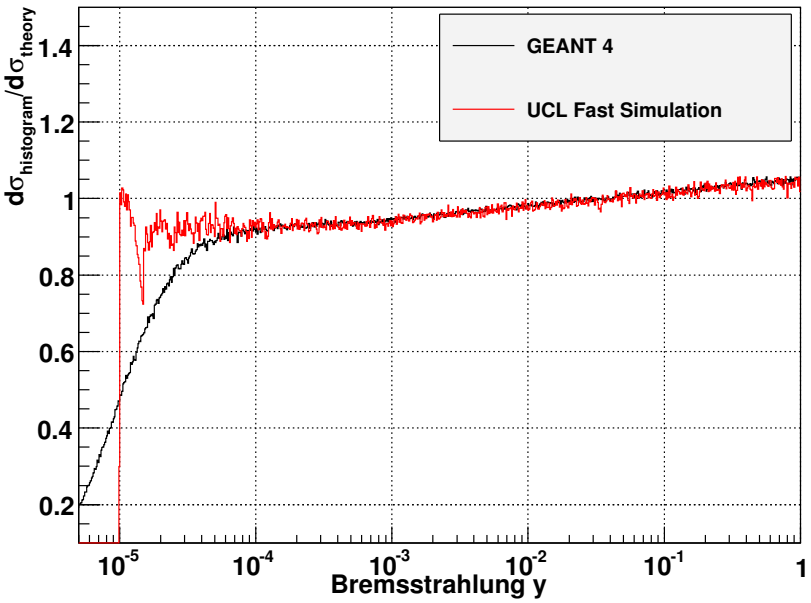

Figure 16: The ratio of GEANT4 and UCL Fast Simulation Modification B Bremsstrahlung y_{eff}-spectra, to the theoretical y spectrum given by 7 with parameterisation B used for low-y suppression. Note the good agreement between GEANT4 and UCL Fast Simulation Modification B in the range $y = 5 \times 10^{-5}$ to $y = 1$, both above and below the LPM cut-off. The reason for discrepancy below $y = 5 \times 10^{-5}$ is unknown. Poor statistics and numerical calculation errors account for the large degree of fluctuation of UCL Fast Simulation Modification B at low-y. UCL Fast Simulation Modification B ratio is zero below $y = 1 \times 10^{-5}$, the minimum value of y it simulates.

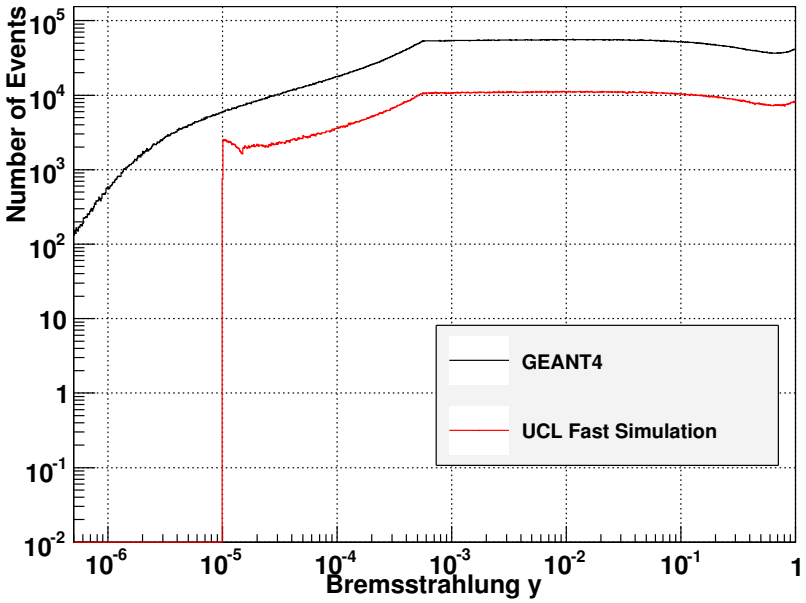

Figure 17: Absolute number of Bremsstrahlung events plotted against y_{eff} for GEANT4 and UCL Fast Simulation Modification B. The GEANT4 curve is greater by an overall scale factor of 5 because it is generated from a larger sample of events. Note that the actual number of events falls considerably at low-y.

be our chosen simulation model. The others will represent models that differ from our chosen model by what we believe is the largest reasonable error on our simulation. We use our chosen simulation model to generate pseudo-data, simulated W boson decay events at a given (realistic) value of m_W. We run the other models to generate W mass likelihood templates and fit to the pseudo-data generated by are chosen model. We take the difference between the fitted m_W and the nominal m_W of the pseudo-data as our systematic error on m_W.

We plan to do this, using UCL Fast Simulation Modification B with a minimum y of $y = 5 \times 10^{-5}$ to generate our pseudo-data. UCL Fast Simulation Modification B with a minimum y of $y = 2 \times 10^{-5}$ and UCL Fast Simulation Modification B with a minimum y of $y = 2 \times 10^{-5}$ reweighted to exactly match the GEANT4 results will be our alternative versions, encompassing any possible errors due to the minimum y and due to the deviation of UCL Fast Simulation Modification B from GEANT4 at very low-y. Unfortunately we are yet to generate sufficient statistics to do this.

An initial estimate of the error was made using numerical integration of the model's spectra combined with various approximations and a small set of pseudo-data. This estimate indicates the error on m_W is of the order of a hundred KeV, which is negligible compared to other sources of error in the W mass analysis.

3.6 Initial Results for Pair Production

Work has been begun on the validation of pair production, the process $\gamma \rightarrow e^- e^+$. The test beam in GEANT4 was changed to a γ beam and the pair production physics process was activated. Bremsstrahlung was deactivated. Again we are interested in energy spectra instead of the total

cross section. The key quantity is

$$x = E/k \tag{24}$$

where E is the energy of the electron produced (or the positron produced - the spectra will always be symmetric), k the energy of the incident photon. The energy of any electron/positron tracks was hence recorded (emerging from either side of the plate), along with that of the the γ. As pair production was only seen in about 1% of cases using a 1 mm thick plate setup, a thicker 1 cm plate setup was used to reduce the overall number of events need to get good statistics on the spectra. 40 GeV photons are uncommon in the W mass analysis, so the the test beam energy was reduced to 5 GeV, an energy more typical of photons simulated in the W mass analysis. A similar setup was used in the UCL Fast Simulation.

Figure 18 compares UCL Fast Simulation and GEANT4's pair production x-spectra to a basic theory curve on a linear scale. The theory curve is plotted according to the following x-spectra,

$$\frac{d\sigma}{dx} = \frac{A}{X_0 N_A}\left(1 - \frac{4}{3}x(1-x)\right) \tag{25}$$

This is taken from reference [11], note the similarity to the Bremsstrahlung spectra given by equation 4 - pair production and Bremsstrahlung are closely related and equations 4 and 25 represent similar limiting cases for the two processes. The overall constant of proportionality was not calculated by enumeration, but instead set to match the scaling of the UCL Fast Simulation histogram by a similar method to that used for Bremsstrahlung theoretical spectra[11]. The spectra appears to agree in the central region in terms of line-shape, however a gap is observed between the GEANT4 and UCL Fast Simulation histograms, possibly due to differences in the way they model the total cross section. The UCL Fast Simulation agrees completely with equation 25 throughout - this is as expected as it samples from this spectrum. GEANT4 significantly deviates for UCL Fast Simulation at high-x and low-x.

The pair production spectrum is expect to have a strong dependence on the energy of the incident photon when this energy is low. The UCL Fast Simulation does not model this. In order to show the effect of this the test beam energy was changed to 100 MeV. Figure 19 compares GEANT4 and the UCL Fast Simulation to the basic theoretical spectra given by equation 25 for a photon test beam of this energy. Note the gap between the histograms has increased considerably, and the region of good agreement in terms of line-shape at the centre is considerably smaller than in figure 18 for 5 GeV.

4 Conclusions and Future Plans

In this report we have shown a validation of the Bremsstrahlung model of UCL Fast Simulation against GEANT4. After appropriate modification of UCL Fast Simulation, guided by examination of the GEANT4 physics model, we have got excellent agreement between the two models over a large range of y values, from $y = 1$ to $y = 5 \times 10^{-5}$. Unfortunately the results found at very low-y were not well understood by us. Here our strategy was to modify UCL Fast Simulation model to be as close as possible to that of GEANT4, and then run virtual test beam experiments to show that we were accurately reproducing the results of GEANT4.

Some differences between GEANT4 and UCL Fast Simulation remained outstanding at very low-y, below $y = 5 \times 10^{-5}$, however initial estimates show these discrepancies only generate a negligible error on the m_W of about 100 KeV. Therefore, pending cross checks, we are confident that the new treatment of Bremsstrahlung in UCL Fast Simulation will be adequate for the Run

[11] Although for Bremsstrahlung we normally scaled the theory to the GEANT4 histogram, not the UCL Fast Simulation histogram.

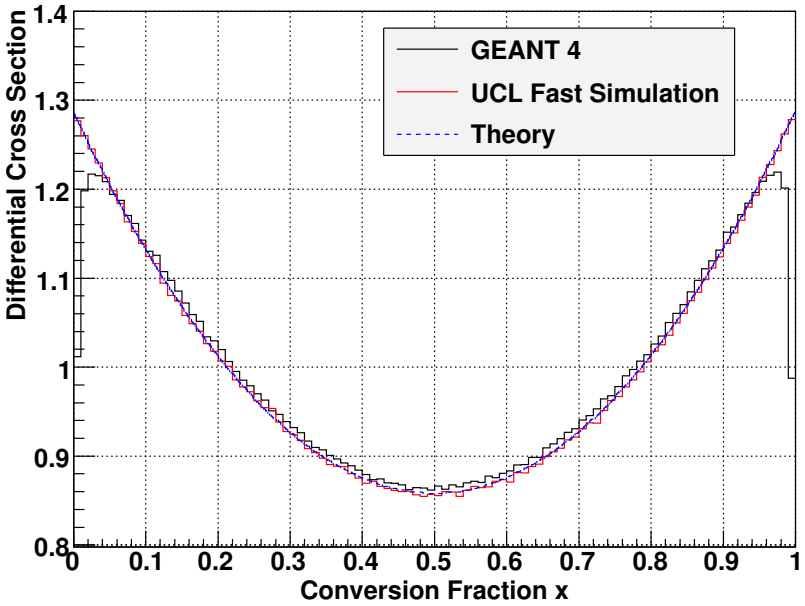

Figure 18: The pair production x-spectra of GEANT4 and UCL Fast Simulation compared to the theoretical x-spectrum given by equation 25 for a 5 GeV test beam of photons. Note the symmetric form, the good agreement in term of line-shape in the central region and the disagreement at low-x and high-x, where UCL Fast Simulation continues to follow the form of 25 while GEANT4 deviates from this considerably. The small gap between the UCL Fast Simulation histogram and the GEANT4 histogram may be due to a difference in the simulation of the total cross section.

.

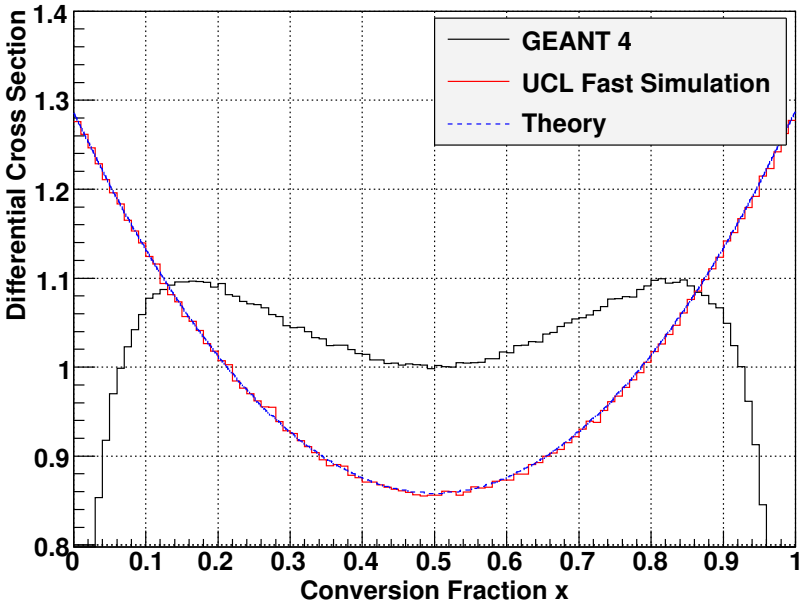

Figure 19: The pair production x-spectra of GEANT4 and UCL Fast Simulation compared to the theoretical x-spectrum given by equation 25 for a 100 MeV test beam of photons. Note the symmetric form, the reduced region (compared to figure 25) of good agreement in terms of line-shape at the centre, and the disagreement at low-x and high-x, where UCL Fast Simulation continues to follow the form of 25 while GEANT4 deviates from this considerably. The gap (increased compared to figure 25) between the UCL Fast Simulation histogram and the GEANT4 histogram may be due to a difference in the simulation of the total cross section.

.

IIb W mass measurement. Given the time constraints of this validation exercise, it is important not to spend time investigating phenomena with no effect on the final value m_W.

As to future plans, a reasonable amount of work is still outstanding on Bremsstrahlung validation. A full error analysis, as detailed in section 3.5 will be performed to check are initial estimates of the an error on m_W of order 100 KeV. Also UCL Fast Simulation Modification B must be further tested at a range of test beam energies, this has already been started but the data was not ready to include in this report. Once this is finished, other energy loss mechanisms in the silicon vertex detector must be investigated, starting with pair production, initial results for which were shown in section 3.6, followed by ionisation and Compton scattering. Plans beyond this will largely depend on outstanding problems in the W mass analysis at the time, but are likely to focus on aspects of the analysis related to UCL Fast Simulation given my experience in the area. It is intended I will transferred to ATLAS at the end of my second year, or thereabouts.

References

[1] M. E. Peskin and D. V.Schroeder, 'An Introduction to Quantum Field Theory', Westview (1995)

[2] D. H. Perkins, 'Introduction to High Energy Physics', 4th Edition, CUP (2000)

[3] Burcham and Jobes, 'Nuclear and Particle Physics', Pearson (1995)

[4] Martin and Shaw, 'Particle Physics', 2nd Edition, Wiley (1997)

[5] T. Aaltonen *et al.* [CDF Collaboration], arXiv:0708.3642 [hep-ex].

[6] LEP Electroweak Working Group, LEP EW WG Plots for Winter 2008 web-page, http://lepewwg.web.cern.ch/LEPEWWG/plots/winter2008/

[7] CDF Public Results Page, http://www-cdf.fnal.gov/physics/physics.html

[8] CDF II Collaboration, FERMILAB-Pub-96/390-E (1996)

[9] K. Amako *et al.*, Nucl.Phys. B, **150**, 44 (2006)

[10] T. Aaltonen *et al.* [CDF Collaboration], Phys. Rev. Lett. **100**, 071801 (2008) [arXiv:0710.4112 [hep-ex]].

[11] W.-M. Yao *et al.*, J. Phys. G **33**, 1 (2006) and 2007 partial update for the 2008 edition available on the PDG WWW pages (URL: http://pdg.lbl.gov/)

[12] S. M. Seltzer and M. J. Berger, Nucl. Instrum. Methods, **B12**, 95 (1985)

[13] Y.-S. Tsai, Review of Modern Physics, **46**, 4, 815 (1974)

[14] GEANT4 Physic Reference Manual, available at http://geant4.web.cern.ch/geant4 /UserDocumentation/UsersGuides/PhysicsReferenceManual/fo/PhysicsReferenceManual.pdf

[15] P. L. Anthony *et al.*, Phys. Rev. D, **56**, 3, 1373 (1997)

[16] A. B. Migdal, Phys. Rev. **103**, 1811 (1956)

[17] J. C. Butcher and H. Messel, Nucl.Phys. **20**, 15 (1960)

[18] V. M. Galitsky and I. I. Gurevich Il Nuovo Cimento, **32**, 2, 1820 (1964)

[19] GEANT4 Source Code, available at http://geant4www.triumf.ca/lxr/